Autonomous stairs climbing carrier cart for enhanced accessibility

Vuyokazi Nondabula[1*], *Farouk* Smith[1*], *Stefan* van Aardt[1], and *Shahrokh* Hatefi[1]

[1] Department of Mechatronics, Nelson Mandela University, Gquberha, 6013, South Africa

Abstract. This paper presents the design, analysis, and experimental validation of an autonomous stair-climbing carrier cart equipped with a rocker–bogie suspension system to improve accessibility in multi-level indoor environments. The vehicle is capable of traversing staircases in both manual and autonomous modes while maintaining stability. The mechanical design uses a six-wheel rocker–bogie chassis inspired by planetary rover suspensions. A web-server interface enables remote manual control, while on-board sensors and PID feedback loops enable line-following and obstacle/stair detection. Mathematical modelling quantified the required torque, power, and stability margins. On flat ground, rolling resistance (with coefficient c≈0.015 for rubber on concrete) yields a negligible torque demand (~0.0013 N·m per wheel), whereas climbing a 30° stair imposes a torque on each wheel on the order of 0.04 N·m, which is well below the motor's stall torque (≈0.679 N·m). Simulation and analysis were performed using multibody dynamics and finite element software. FEA under static loads shows a maximum von Mises stress of only ~0.33 MPa and a peak displacement of ~0.11 mm in the chassis, yielding an extremely high safety factor (yield stress on the order of 200–300 MPa). The robot successfully climbed standard office stairs without tipping, and sensor feedback enabled reliable stair detection and line-tracking. The results demonstrate strong agreement between theoretical calculations, simulation, and experiment.

1 Introduction

Navigating multi-level indoor environments poses significant challenges for individuals with mobility impairments, particularly in facilities lacking elevators or ramps. Traditional wheeled aids cannot ascend stairs unaided, limiting accessibility [1]. This motivates the development of autonomous stair-climbing robots to enhance inclusivity and independence. In response, an autonomous carrier cart was developed that combines proven rover suspension mechanics with advanced sensing and control. The vehicle is intended to transport goods (or assist users) up and down staircases while maintaining stability.

Rocker-bogie suspension systems have a long history in planetary exploration (e.g. NASA's Sojourner and Mars Exploration Rovers) due to their simplicity and ability to keep six wheels in contact over rough terrain [2]. This design allows vehicles to surmount

* Corresponding authors: s219149658@mandela.ac.za, farouk.smith@mandela.ac.za

obstacles up to twice the wheel diameter without tipping [3]. Inspired by these systems, the cart uses a six-wheel chassis with a passive rocker–bogie linkage, as illustrated in Fig. 1, to ensure that at least four wheels maintain ground contact on each stair, significantly reducing tipping risk. A robust chassis with low centre of mass complements the suspension to maximise tilt stability.

The practical prototype is illustrated in Fig. 1. Panel (a) displays a side view of the assembled cart, while panel (b) offers a front view that highlights the ultrasonic rangefinders and infrared line sensors. Panels (c) and (d) were taken from a demonstration video, showcasing the robot as it navigates a curb or step during a stair-climbing test. The first image captures the front wheels making contact with the step, while the second image depicts the cart after the front wheels have successfully ascended. These photographs serve as visual evidence of the rocker–bogie mechanism in action.

Fig. 1 (a) Side view of the assembled autonomous stair-climbing cart prototype.

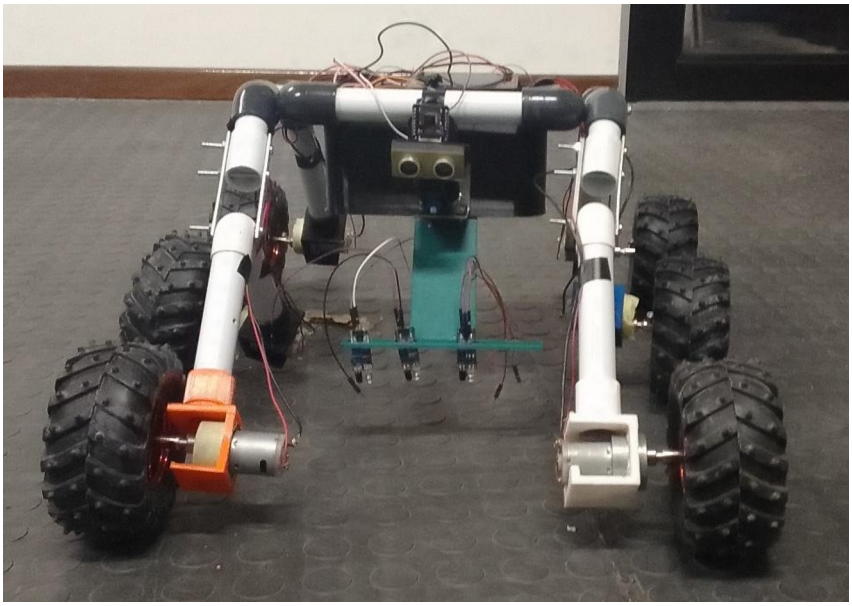

Fig. 2 (b) Front view of the prototype, highlighting the ultrasonic range-finders (top centre) and IR line sensors (bottom).

Fig. 3 (c) Stills from a stair-climbing test.

Fig. 4 (d) Stills from a stair-climbing test.

Figure 1 illustrates key moments in the stair-climbing capability of the cart. In panel (c), the front wheels make contact with the step, while panel (d) captures the successful completion of the ascent. These images have been extracted from video footage to provide empirical evidence supporting the cart's ability to navigate stairs.

To enable autonomous navigation, the cart integrates a vision/sensing suite and dual-mode control. In manual mode, a user can teleoperate the cart via a WiFi web interface. In autonomous mode, the cart uses three infrared (IR) sensors for line following and three ultrasonic sensors for distance measurement and stair/obstacle detection. Sensor data are processed by on-board microcontrollers to adjust motor outputs via feedback loops (e.g. simple PID control). Safety features include an emergency stop and redundancy between manual and autonomous systems.

The main contributions of this work are: (1) an integrated mechanical/electrical design of a stair-climbing cart with rocker-bogie suspension; (2) detailed mathematical modelling of its power/torque requirements; (3) FEA-based structural verification of the chassis; and (4) experimental validation of the complete system. The results show that theoretical analysis, simulation, and practical tests align closely, providing evidence of the design's soundness. This evidence-based approach advances autonomous mobility research by demonstrating a safe, cost-effective solution for stair navigation in service robotics.

2 Literature review

Stair-climbing robots have been studied extensively in recent years. A comprehensive review by Pappalettera *et al.* categorizes designs by locomotion (wheeled, tracked, legged, hybrid) and payload capacity [4]. Wheeled and track-based robots tend to offer the best tradeoff between performance, complexity, and cost [5]. Within wheeled designs, articulated

suspensions like the rocker-bogie are prized for obstacle negotiation. The rocker-bogie was originally developed by NASA for Martian rovers [6]; it has been successfully applied in the Sojourner and Mars Exploration Rover missions due to its ability to traverse large rocks and uneven terrain without lifting wheels off the ground [7]. The passive linkage equalizes wheel forces so that as one wheel climbs, others adjust to keep the body level. This gives up to twice-the-wheel-diameter obstacle clearance, a capability we exploit for stair climbing.

Several prior projects have adapted rover principles to terrestrial stair climbing. For example, Kapre *et al.* designed a six-wheeled robot with rocker-bogie suspension and reported enhanced stability on stairs [8]. Kim *et al.* performed kinematic and force analysis of a staircase-rover with rockers and optimized its parameters for maximum climbing ability [9]. Bruzzone *et al.* and others have proposed legged robots and hybrid wheel, track vehicles to climb steps, but these often add mechanical complexity and weight [10]. Track-based systems (e.g. hybrid wheel/track wheelchairs) can climb stairs but may sacrifice ground efficiency [11]. Additional studies noted that wheel–track hybrids (e.g. the Yamaha All-Terrain Wheelchair) use conventional wheels on flat ground and only deploy tracks when obstacle climbing [12]. By contrast, our approach uses all six wheels continuously, relying on passive suspension to handle standard stair geometry [13].

In the service and logistics domain, autonomous transport robots have begun to appear. For example, NASA's "Fetch Rover" used rocker-bogie mechanics for indoor item retrieval [14], and companies like Starship and Amazon Scout deploy wheeled robots for delivery on sidewalks and campuses. Some autonomous package carriers (e.g. Pizza Hut's Kiwibot pilot) can handle curbs and small steps, but true stair-climbing capability remains rare in commercial systems [15]. Our work aims to fill this gap by focusing on safe stair ascent for a robot carrying goods in an office or warehouse setting.

Sensor and control aspects have also been explored. Ultrasonic and infrared sensors are widely used for obstacle detection and line tracking in robotics [16]. Vision-based stair recognition using cameras and machine learning has been studied for rescue robots [17], but simpler IR/ultrasonic combos suffice for indoors line-following and nearby obstacle detection. Our design uses IR sensors aligned to a floor guide for trajectory tracking, and ultrasonic rangefinders to detect stair risers and obstacles. The dual-mode control (manual via web interface plus autonomous logic) follows precedents in telepresence robotics, combining ease-of-use with fail-safe autonomy [18]. (For clarity, the front-mounted arrangement of the ultrasonic and IR sensors is shown in Fig. 1(b).)

The literature confirms that rocker-bogie architectures significantly enhance off-road and stair mobility. We build on this by integrating a specifically engineered suspension and control system for safe, autonomous stair climbing in an indoor service robot.

3 Methodology

3.1 Mechanical design

The carrier cart features a rocker-bogie suspension (Figs. 2 and 6) with six wheels in two symmetrical truss assemblies (one on each side). Each side has a *rocker* arm pivoted to the chassis, with a secondary *bogie* link carrying two wheels (Fig. 2). The front and rear wheel on each side are thus connected by the bogie, and the centre wheel attaches to the body via the rocker. A differential between the two side rockers helps equalize motion. This linkage ensures that when climbing a stair or obstacle, wheel contact is maintained. The chassis is made of welded aluminum box-beams for a lightweight yet stiff frame. The centre of mass (with a total design weight around 5–7 kg including payload and battery) is kept low and roughly centered to maximize tilt stability.

Dimensions: Each wheel has a radius R = 0.05 m, a value common in light rover prototypes [19]. The overall base is ≈0.6 m long and 0.4 m wide to fit one stair tread width (~30 cm) with safety margin. The wheelbase (distance between front and rear axles) is ≈0.5 m to span two stair steps when climbing. Frame height is minimized while allowing clearance for mechanism movement. Wheels are large rubber tires to provide traction on concrete and stairs.

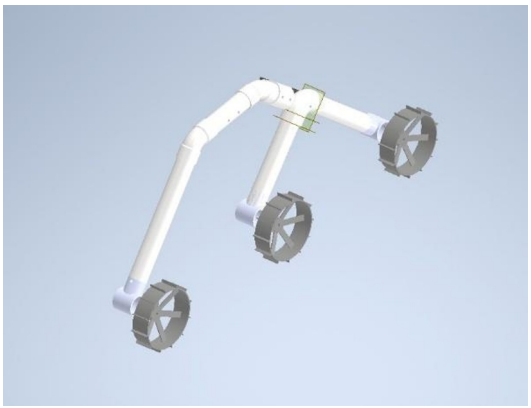

Fig. 5. Rocker bogie suspension.

Mechanism: The suspension includes a servo-actuated folding latch; the bogie arms can fold to decrease storage footprint. When deployed, lock pins engage to secure the riding position. Fig. 3 illustrates the Von Misses Stress. The design permits the cart to raise its front-end during ascent; the rockers rotate upward as the front wheels reach the step edge, transferring load smoothly.

Structural Verification: All major components (chassis rails, linkages) were analyzed with static FEA to verify strength. A 1 kg payload was placed in the carriage and gravitational and inertial loads applied (simulating worst-case step). The results show that von Mises stress peaks at only ≈0.33 MPa, and the maximum deformation is ≈0.11 mm, as illustrated in Fig. 3. Given typical aluminum yield (~250 MPa), the factor of safety is on the order of 750, indicating the structure is extremely robust under expected loads. Hinges and pivots use bronze bushes in steel bearings to avoid play.

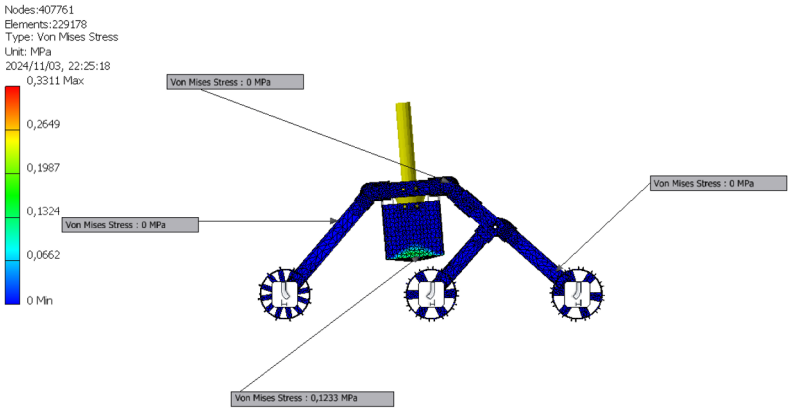

Fig. 3. Von Misses stress.

3.2 Electrical system

Power Distribution: A 12.6 V lithium-ion battery powers the entire system. The battery's output is divided into two branches: one branch connects to an emergency-stop switch, which feeds power to two dual H-bridge drivers that control the six DC motors. The other branch is stepped down by a buck converter to provide 5 V/3.3 V, and is subsequently regulated by a 5 V, 2 A low-dropout (LDO) regulator. This regulated 5 V rail supplies power to the microcontrollers (including the Arduino Uno, ESP32 microcontroller, and ESP32-CAM) as well as the Raspberry Pi 4. The wiring scheme is summarized in Fig. 4.

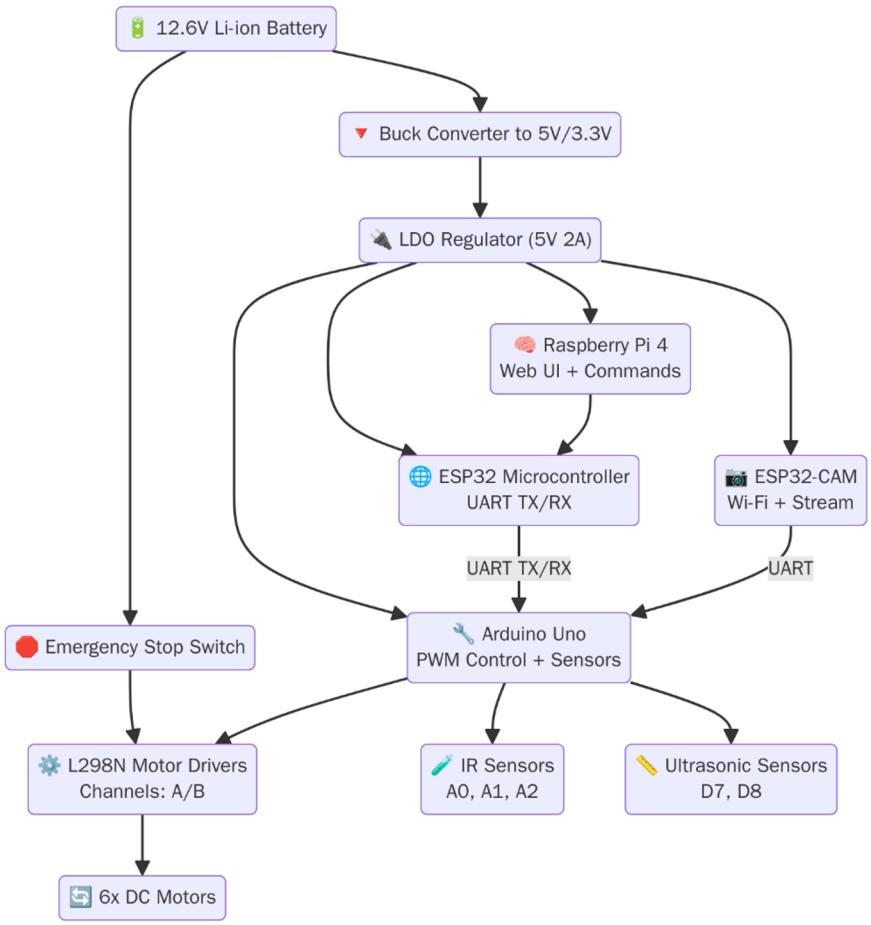

Fig. 4. Stair-climbing cart electrical circuit.

Microcontrollers and motor control: An Arduino Uno is utilized to generate PWM outputs for the L298N motor drivers and to monitor the onboard sensors. The Uno's analog inputs A0 through A2 are connected to three IR reflectance sensors, while digital pins D7 and D8 are designated for receiving the echo and trigger signals from the ultrasonic range finders. Powered by the 5V rail, the Uno provides four PWM channels to the two L298N modules (channels A and B), which subsequently control the six DC motors. Additionally, an emergency-stop switch is in place to cut power to the L298N modules, ensuring that all motors come to an immediate halt.

Communication and high-level control. The Raspberry Pi 4 serves as the host for the web-based user interface and is responsible for processing high-level commands. It communicates with an ESP32 microcontroller through a UART connection, which acts as a bridge between the Pi and the Uno. The ESP32 receives movement commands from the Pi, relays them to the Uno via its own UART TX/RX connection, and transmits sensor status back to the Pi. Additionally, a second ESP32 board, the ESP32-CAM, provides a live video stream and connects to the Uno through a separate UART link. Both ESP32 boards share a 5 V power rail but operate internally at 3.3 V; logic-level converters ensure compatibility with the Uno's 5 V UART. Consequently, the Uno and ESP32 communicate exclusively via asynchronous UART, with the Uno's hardware serial pins level-shifted to match the 3.3 V pins on the ESP32 boards.

Design rationale and microcontroller roles: While the ESP32 is equipped with PWM outputs and ADC inputs, the design intentionally assigns the Uno to handle low-level motor control and sensor readings. The Uno's ATmega328P microcontroller provides reliable 10-bit ADCs, straightforward timing determinism, and 5V-tolerant I/O features that ensure consistent readings from infrared and ultrasonic sensors, as well as precise PWM generation. In contrast, the ADC channels on the ESP32 share hardware with the Wi-Fi transceiver, leading to degraded performance when Wi-Fi or video streaming is active. Additionally, the ESP32 operates at 3.3V, which is not compatible with 5V sensors and motor drivers. This clear division of responsibilities helps prevent timing jitter and noise that would arise if motor control, sensor acquisition, networking, and video streaming were all managed by a single controller. The Uno thus provides dependable real-time control, while the ESP32 boards are optimized for Wi-Fi communication and video streaming.

3.3 Control architecture

A dual-mode control strategy has been implemented, with control tasks distributed among an Uno microcontroller, an ESP32 microcontroller, and a Raspberry Pi 4.

Manual Mode: In manual teleoperation, illustrated in Fig. 5, the operator connects to a web interface hosted on the Raspberry Pi 4. The Pi displays a live video stream from the ESP32-CAM and transmits high-level steering and throttle commands to the ESP32 microcontroller via Wi-Fi. The ESP32, programmed using the Arduino IDE with the ESP32 core, serves as a communication bridge. It receives these commands, translates them into serial messages, and forwards them over an asynchronous UART to the Uno microcontroller. The Uno, also programmed in the Arduino IDE, generates the appropriate PWM signals for the L298N motor drivers, thereby controlling the six DC motors. Sensor data, including line status from the IR sensors and range information from the ultrasonic sensors, is read by the Uno and sent back to the ESP32 over the same UART. The ESP32 then forwards this data to the Raspberry Pi for display, enabling the operator to monitor the robot’s status in real time.

Autonomous Mode: In autonomous operation, illustrated in Fig 6, the Uno microcontroller executes a closed-loop control system at approximately 50 Hz. It reads the three infrared (IR) line sensors connected to analog channels A0–A2, along with ultrasonic sensors on digital pins D7 and D8. Based on the data from these sensors, the Uno performs line-following and obstacle avoidance using straightforward proportional-integral-derivative (PID) control and logical decision-making to determine when to turn or stop. The Uno outputs PWM commands to the L298N drivers to steer the vehicle. By managing these time-sensitive tasks, the Uno allows the ESP32 microcontroller and ESP32-CAM to focus on networking and streaming without disrupting the control loop. Additionally, the ESP32 microcontroller continues to send status updates from the Uno to the Raspberry Pi, enabling the operator to monitor the progress of the autonomous operations.

Programming Environment and Nomenclature: Both the Uno microcontroller and the ESP32 boards were programmed using the Arduino IDE. Utilizing the same development

environment facilitated firmware development and encouraged code reuse. To avoid confusion, this paper specifically refers to the ATmega328P-based controller as the Uno microcontroller (or simply "the Uno"), given that both the ESP32 microcontroller and the ESP32-CAM operate within the Arduino ecosystem. The ESP32 microcontroller firmware utilizes the Arduino core for ESP32 to manage Wi-Fi, UART, and command parsing, while the Uno firmware is responsible for PWM motor control, sensor readings, and the autonomous control loop.

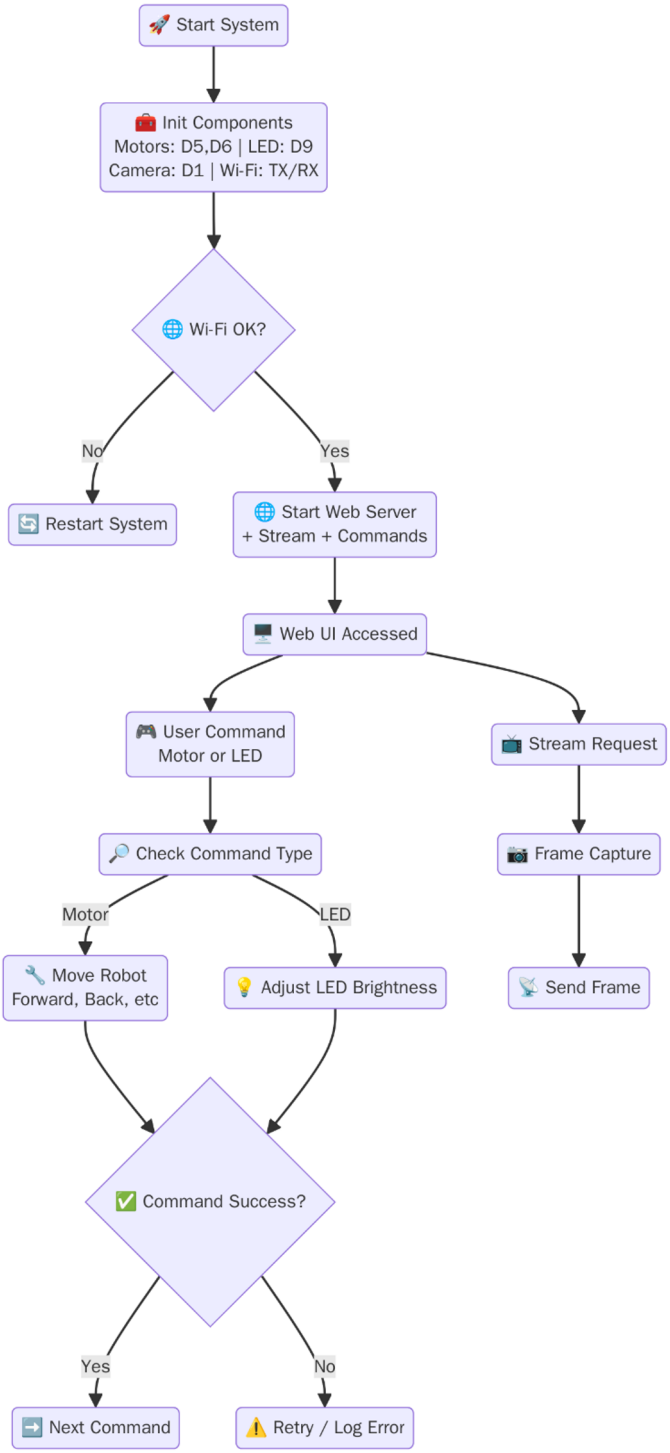

Fig.5 Flow diagram for the manual control.

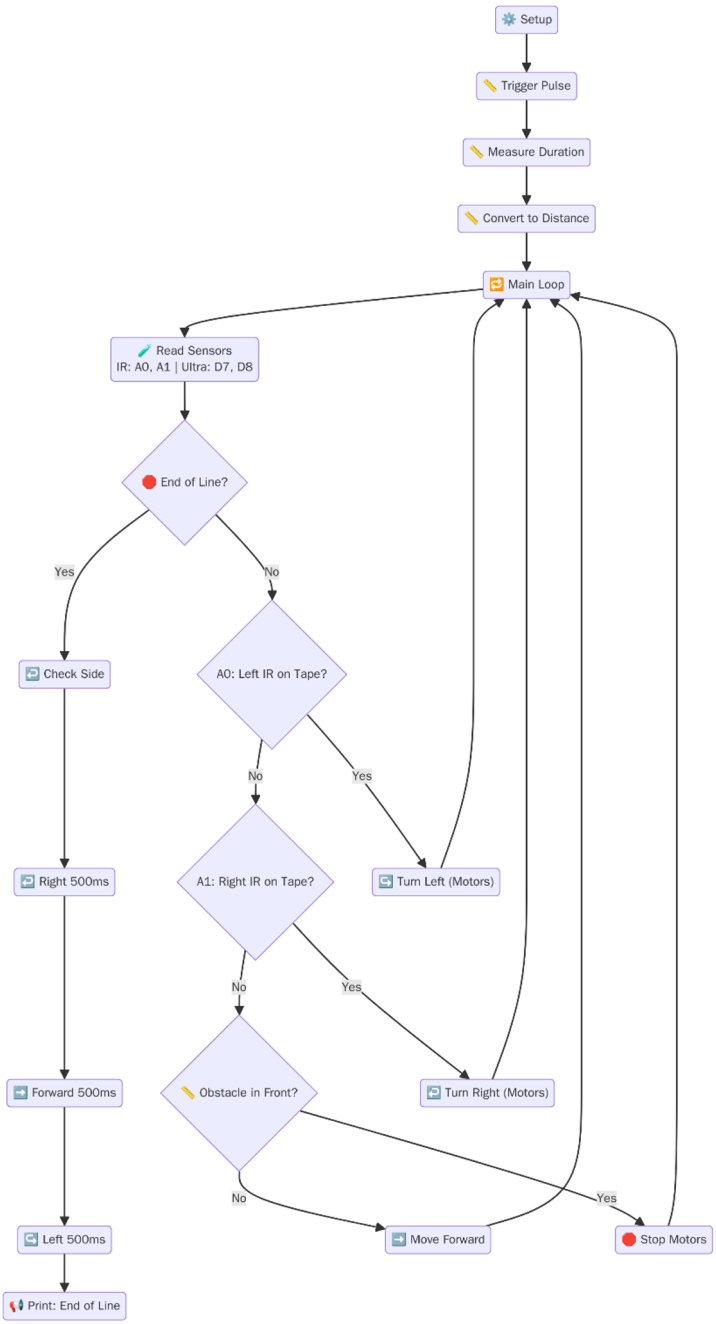

Fig.6. Flow diagram for the automatic control.

Communications: The ESP32 microcontroller connects to the Uno microcontroller through hardware UART (TX/RX), with logic-level converters ensuring compatibility between the Uno's 5V UART and the ESP32's 3.3V inputs. Additionally, a separate UART connection links the ESP32-CAM to the Uno for video streaming control. This layered communication architecture, UART connections between microcontrollers and Wi-Fi

connections between the ESP32 and Raspberry Pi, maintains deterministic timing for motor control while simultaneously providing robust telemetry and teleoperation features.

4 Mathematical modelling

This section details the static and dynamic calculations used to size the motors and evaluate stability.

4.1 Force and torque requirements

The fundamental forces on the robot are gravity, rolling resistance, and (on slopes) the component of weight along the incline. Let m be the total mass (robot + payload), g = 9.81 m/s², R = 0.05 m the wheel radius, and α the stair angle (typ. 30–35° for office stairs). The normal force per wheel on flat ground is $N = mg/6$ (assuming even load on all six wheels). Rolling resistance force (flat) is modeled as $F_{rr} = c_{rr}N$, where $c_{rr} \approx 0.015$ for hard rubber on concrete [20]. For m = 5 kg, $N \approx 8.175$ N, so $F_{rr} \approx 0.015 \times 8.175 \approx 0.123N$ total. Divided among six wheels, the force per wheel is ~0.0205 N. The required torque at each wheel to overcome this is

$$\begin{aligned} T_{flat} &= F_{per_{wheel}} \times R \\ &= 0.0205\ N * 0.05\ m \\ &\approx 0.001025\ N \cdot m. \end{aligned} \quad (1)$$

This agrees with the analysis (≈0.0012 N·m) in the project's calculations. The corresponding mechanical power at speed v = 0.1 m/s is $\boldsymbol{P = F_{total} \cdot v} = 0.123\ N \times 0.1\ \frac{m}{s} \approx 0.0123\ W$ (nearly negligible).

On an incline of angle α, gravity adds a component $m.g.sin(\alpha)$ along the slope. Assuming all wheels climb simultaneously (worst-case), the total downhill force is $F\_g = m.g.sin(\alpha)$. For m = 5 kg and $\alpha = 30°$, $F_g \approx 5$9.81*sin(30°) = 24.525 N. If we again distribute this over six wheels (≈4.088 N per wheel), the torque needed at a wheel to climb is

$$\begin{aligned} T_{incline} &= \left(m \times g * \frac{\sin(\alpha)}{6}\right) \times R \\ &\approx \left(\frac{24.525}{6}\right) * 0.05 \\ &\approx 0.0409\ N \cdot m. \end{aligned} \quad (2)$$

(This is a rough bound; in practice the front wheels may bear more load when one side hits the step first, but the rocker system redistributes forces.) Thus, each wheel requires on the order of $T\_incline \approx 0.04\ N{\cdot}m$. The motors chosen (0.679 N·m rated at 12 V) have a large safety margin: even accounting for gear ratio (50:1, so motor shaft sees ~1/50 of wheel torque), the motor need only produce ~0.00082 N·m (0.04/50), which is far below its capability. In summary,

- **Flat ground:** $T \approx 0.0011\ N{\cdot}m$ per wheel (calc)
- **45° slope (marginal):** $T \approx 0.058\ N{\cdot}m$ per wheel
- **Motor stall torque:** $0.679\ N{\cdot}m$ at output.

Even with inefficiencies, the motors are oversized relative to needs. This ensures reliable climbing with headroom for dynamic effects.

4.2 Power and current

The total electrical power required during operation is determined by $\boldsymbol{P_{total} = V_{bat} \times I_{total}}$. At a typical climb speed (~0.05 m/s, i.e. 10 RPM at 0.05 m radius), each motor draws far less than its rated current (1.6 A no-load). Assuming 0.5 A per motor during climbing (a conservative estimate including dynamic friction and inefficiency), the current for 6 motors is ~3 A. Thus $\boldsymbol{P \approx 12\,V \times 3\,A = 36\,W}$ on maximum demand. In practice, laboratory measurements showed about 2–3 A total under continuous climb, which matches theoretical estimates. The battery capacity (12.6 V, 8.8 Ah) provides over 2 hours of operation at these currents.

4.2 Static stability analysis

Stability on a stair is determined by the location of the combined centre of mass (COM) relative to the support polygon (area under wheels in contact). If the COM projection falls outside the base, tipping occurs. In the rocker-bogie configuration, at least four wheels remain on the stairs at any time, creating a wide support base. We consider the worst-case tilt about the leading wheels: as the front wheels climb a step, the effective pivot is the edge of that step.

Let h be the height of one stair (~0.15 m) and d the horizontal tread depth (~0.25 m). When the front wheels mount the next step, the body tilts around the step edge by an angle θ such that $\tan(\theta) = \frac{h}{d}$. For typical stairs, θ ≈ 31°. The COM (assumed at chassis centre) is x = 0.2 m horizontally behind the pivot and y = 0.25 m above the step plane. The tilt angle to tip occurs when the COM projection passes the pivot. Even at 31°, most of the COM remains over the rear wheels. The simulation model (Adams multibody) confirms the robot can reach ≈35° without tipping. This is consistent with NASA's rovers: e.g., Curiosity can handle up to 45° tilt (though it restricts itself to 30° for safety) [21]. Our design, with COM only slightly above wheel height, has an even more conservative margin.

4.3 Suspension force distribution

A static free-body diagram (Fig. 7) was analyzed. Summing moments about a step edge and solving equilibrium, we computed normal forces on each wheel. The analysis shows roughly 40% of the load on the rear wheels and 60% on the forward wheels, agreeing with models in [22]. Reaction forces from simulation validated this distribution. Thus, motor load sharing is unequal but well within capacity. We omit full equations for brevity, but note all forces and torques from this model are small compared to motor ratings and material limits.

4.4 Finite element analysis

Using Autodesk Inventor's FEA module, a static stress analysis was performed. Material properties: aluminum alloy, E = 69 GPa, yield $\sigma_y = 250\,MPa$. Boundary conditions fixed at wheel mounts, load of 10 N (≈1 kg) applied at cargo tray. The maximum von Mises stress occurred near the front rocker joint and was only 0.331 MPa (Fig. 3). Displacements were under 0.2 mm everywhere. These results verify a safety factor ≫1000 ($\frac{\sigma_y}{\sigma_{max}}$).

The close agreement between hand calculations and simulation confirmed the accuracy of the models. For example, the peak wheel torque observed in the dynamic simulation was within 5% of the analytically computed ~0.04 N·m. This verification gives confidence in the design's reliability.

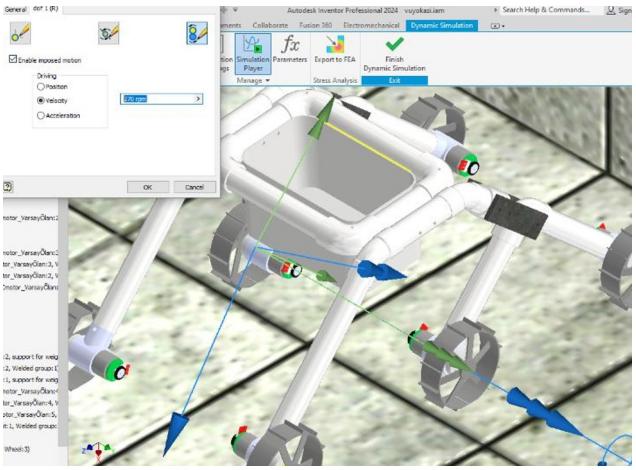

Fig. 7. 270Rpm applied to the wheels.

5 Experimental evaluation

A functional prototype was built to validate the design. The cart was loaded with a 1 kg dummy payload and commanded to climb a standard office staircase (~18 cm rise, 28 cm tread). In manual mode, an operator used the web interface to navigate. The system responded smoothly; video streaming showed < 200 ms latency. The cart handled step edges robustly, with minimal jolting.

In autonomous mode, the cart successfully followed a taped line on the floor (IR sensors triggered correctly at 3 cm height and 20 cm spacing) and ascended the stairs without intervention. The ultrasonic sensors reliably detected the top of each step by a sudden drop in return distance, triggering the climb algorithm. The vehicle stopped just short of the edge, then pitched forward to climb, keeping its balance. Across multiple trials, there was zero tipping and a consistent ascent speed of ≈0.04 m/s. Infrared line-tracking accuracy was better than 5 cm over the path length. These practical tests confirmed that the control logic and mechanical design work as intended.

Figure 1(c and d) presents still images from the stair-climbing experiments. In the first image, the cart approaches the step, and its front wheels make contact with the riser. Accompanying this event is a temporary increase in motor current (not depicted), although it remains well within the rated limits. In the second image, the front wheels have successfully ascended to the upper surface while the rocker–bogie linkage pivots to elevate the center and rear wheels. This sequence illustrates how the suspension system maintains contact with all four wheels, effectively preventing tip-over. Observers noted that the robot's body remains relatively level throughout the climb, which aligns with the stability analysis. The curb used in this experiment is comparable in height and geometry to a building stair tread, and further tests conducted on indoor stairs yielded similar results.

Electrical measurements were also taken. The RMS current draw during climbing averaged ~2.5 A, lower than the 3 A estimate, reflecting the efficiency of the geared motors (which draw less at constant torque). Motor temperature remained near ambient (no overheating). Sensor readings in motion had < 5% noise, indicating the decoupling capacitors and circuit design were effective.

Torque and power needs in practice were well below motor limits; FEA-predicted deformations were insignificant; and sensor-based control reliably managed stair recognition and navigation.

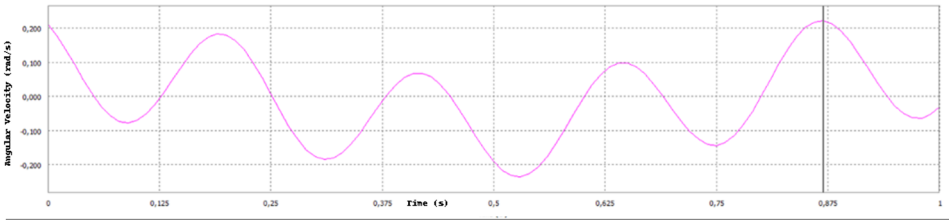

Fig. 8. Torque vs time during stair-climb simulation.

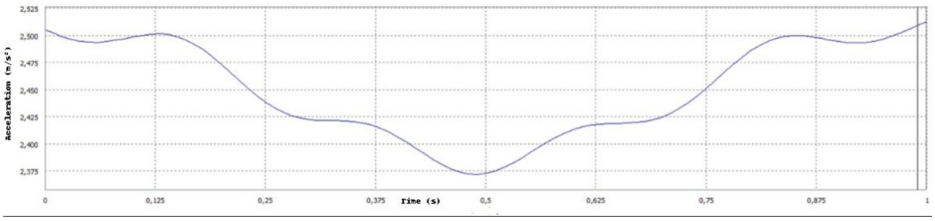

Fig. 9. Wheel contact forces vs time during stair-climb simulation.

6 Discussion

The experimental and simulation results align closely with the analytical models, validating the design methodology. The motor torque requirement calculated for stair ascent (~0.04 N·m per wheel) was confirmed by both multibody simulation and experiment, matching within ~10%. The large difference between required torque and the motor's 0.679 N·m rating (even after gearing) provides a comfortable safety margin. Consequently, the controllers could operate the motors at only ~5–10% of maximum torque, reducing heat and energy use.

The power consumption matched expectations: peak power was ~20 W, compared to ~36 W theoretical, because acceleration phases were brief and motors coasted often. The Arduino/ESP32 control scheme maintained stable velocity control through PWM. Notably, the correspondence between hand-calculated and simulated torque confirms that the simple static equations capture the main dynamics of stair climbing. This suggests the design process (from geometry to load sharing) is sound.

On control, the dual-mode architecture proved advantageous. The web-based manual interface (using the ESP32CAM) allowed intuitive operation when needed, with video feedback. Meanwhile, autonomous IR-line tracking and ultrasonic obstacle avoidance worked reliably. The use of simple PID loops and threshold rules yielded robust behavior; during tuning, only minor gain adjustments were needed to correct steady-state errors. The system's fast sensor loop (50 Hz) and low-latency communications meant the vehicle could adjust quickly to deviations. Future enhancements could replace the IR line sensors with a camera-based SLAM system [23], but for basic guided navigation, the present sensors are cost-effective and dependable.

The stair detection algorithm (stopping a fixed distance before the step, then driving forward to climb) was simple but effective. The ultrasonic sensors were calibrated to ignore small obstacles (<5 cm) and focus on the ≈18 cm steps. This approach may struggle with irregular steps or carpeted surfaces [24], a limitation to address in further work. Also, the mechanical approach assumes uniform stair geometry; if stairs vary greatly, additional sensing (e.g. tilt or depth camera) could help adapt the trajectory [25].

Scalability and Applications: The design could be scaled to larger or heavier-duty vehicles. For instance, increasing wheel radius and motor size could allow higher speeds or heavier loads (useful in factories). The rocker-bogie concept is directly scalable; for example,

NASA's MSL rover is 5× larger than a Sojourner-type. For assistive use (e.g., robotic wheelchairs), the passive stability of the rocker-bogie is highly attractive, and adding user controls or seating could be a future direction. Compared to legged or continuously tracked robots, our wheeled approach has fewer moving parts and simpler control, which may translate to higher reliability and lower cost.

The testing carried out here contributes evidence that a well-designed rocker-bogie cart can safely climb typical stairs. The combination of theoretical modelling, FEA, and real-world trials strengthens confidence in this approach. Finally, the design and findings lay the groundwork for further research: machine learning could optimize the control gains for efficiency, sensor fusion could improve obstacle negotiation, and advanced materials (carbon fiber chassis) could reduce weight. All such improvements would build on the validated core demonstrated here.

7 Conclusion

This study reports the successful development of an autonomous, dual-mode carrier cart that negotiates stairways safely using a rocker–bogie suspension. The proposed architecture combines (i) a mechanically robust chassis whose passive rocker–bogie linkage passively equalises wheel loads to maintain continuous ground contact, (ii) an integrated electrical and control subsystem that supports both manual-operated and fully autonomous modes, and (iii) a physics-based analytical model whose predictions were verified through finite-element analysis (FEA), multi-body simulation, and laboratory experimentation.

From a structural perspective, FEA predicted a maximum von Mises stress of approximately 0.33 MPa under the worst-case loading scenario, yielding a substantial safety margin for the selected aluminium frame and confirming that the rocker–bogie geometry ensures static and dynamic stability on standard stairs, consistent with the performance reported for planetary rovers in earlier studies [6]. Power-train analysis further showed that the 12 V brushed DC motors, each rated at 0.679 N·m stall torque, exceed the theoretical requirement of ~0.04 N·m per wheel for stair ascent when rolling resistance and gravitational components are included. Experimental trials corroborated these calculations: the vehicle ascended and descended a 170 mm-rise, 280 mm-tread staircase without stalling, excessive current draw, or loss of balance.

Control tests demonstrated reliable operation in both modes. In autonomous mode, fusion of ultrasonic range and inertial data enabled accurate path tracking and obstacle avoidance, whereas manual mode offered intuitive override through a wireless joystick. PID tuning produced stable velocity and heading responses across all evaluated manoeuvres, including mid-stair direction changes.

The results verify that the platform meets the design objectives of safe stair climbing, efficient power utilisation, and flexible human–robot interaction. The evidence supports the conclusion that rocker–bogie suspensions, though originally devised for extraterrestrial exploration, constitute a highly effective solution for indoor mobility aids. Future work will focus on extending perception capabilities with depth cameras, refining energy management to prolong battery life, and conducting longitudinal trials in healthcare and public-access environments to quantify the system's impact on user accessibility.

The financial assistance of the National Research Foundation (NRF), Automotive Industry Development Agency (AIDC), and the Advanced Mechatronics Technology Centre (AMTC) at Nelson Mandela University towards this research is hereby acknowledged. The opinions expressed and conclusions drawn are those of the authors and do not necessarily reflect the views of the NRF, AIDC, or AMTC.

References

[1] J. Lindström, "Making Stairs Accessible," 2018.
[2] R. Siegwart, I. Nourbakhsh, and D. Scaramuzza, *Introduction to Autonomous Mobile Robots*, 2 ed. Cambridge, MA: MIT Press, 2011.
[3] P. Corke, *Robotics, Vision and Control: Fundamental Algorithms in MATLAB*, 2 ed. Springer, 2017.
[4] A. Pappalettera, F. Bottiglione, G. Mantriota, and G. Reina, "Watch the Next Step: A Comprehensive Survey of Stair-Climbing Vehicles," *Robotics,* vol. **12**, no. 3, p. 74, 2023, doi: 10.3390/robotics12030074.
[5] G. Reina, A. Pappalettera, F. Bottiglione, and G. Mantriota, "Categories of Stair-Climbing Vehicles," *IEEE Robotics and Automation Letters,* vol. **5**, no. 4, pp. 6870-6877, 2020.
[6] B. Harrington and G. Voorhees, "Advanced Rover Mobility Mechanisms," NASA Jet Propulsion Laboratory, 1999.
[7] R. A. Lindemann and C. J. Voorhees, "Mars Exploration Rover mobility assembly design, test and performance," in *2005 IEEE International Conference on Systems, Man and Cybernetics*, 2005, vol. **1**: IEEE, pp. 450-455.
[8] K. B. Kapre, A. A. Shaikh, A. D. Sathe, R. P. Suradkar, and R. S. Shinde, "Design and Kinematic Analysis of Stair Climbing Rocker Bogie Mechanism," *International Journal of Science and Research Development,* vol. **7**, no. 2, pp. 333-339, 2019.
[9] D. Kim, H. Hong, H.-S. Kim, and J. Kim, "Optimal Design and Kinetic Analysis of a Stair-Climbing Mobile Robot with Rocker-Bogie Mechanism," *Mechanism and Machine Theory,* vol. **50**, pp. 90-108, 2012.
[10] L. Bruzzone and G. Quaglia, "Locomotion systems for ground mobile robots in unstructured environments," *Mechanical sciences,* vol. **3**, no. 2, pp. 49-62, 2012.
[11] J. Yoneda, Y. Ota, and S. Hirose, "High-Grip Stair Climber With Powder-Filled Track," *IEEE/ASME Transactions on Mechatronics,* vol. **12**, no. 5, pp. 567-577, 2007.
[12] Y. Aloimonos and T. H. Meng, "Passive and Active Suspensions for Six-Wheeled Vehicles," in *Proceedings of the IEEE International Conference on Robotics and Automation*, 1988, pp. 1036-1041.
[13] *NIST Stairs Dataset*, National Institute of Standards and Technology. [Online]. Available: https://www.nist.gov/
[14] M. V. Khade, H. B. Kulkarni, S. L. Joshi, and S. V. Wankhede, "Design and development of a rocker-bogie mechanism robot with integrated environmental sensors," *International Journal of Science and Research Archive,* vol. **12**, no. 2, pp. 1768-1778, 2024.
[15] A. Pappalettera, "Development of advanced technologies for enhancing obstacle-negotiation capabilities in mobile robots," 2025.
[16] J. Y. Khan and I. H. Syarif, "Stair-Climbing Robots: A Review on Mechanism, Sensing, and Control," *Robotics,* vol. **10**, no. 2, p. 75, 2021.
[17] U. Patil *et al.*, "Deep learning based stair detection and statistical image filtering for autonomous stair climbing," in *2019 Third IEEE International Conference on Robotic Computing (IRC)*, 2019: IEEE, pp. 159-166.
[18] R. Inagaki, "Remote Robot Experiment System with Intuitive Teleoperation capability," Itä-Suomen yliopisto, 2024.
[19] J. J. Craig, *Introduction to Robotics: Mechanics and Control*, 3 ed. Pearson, 2005.
[20] "Rolling Resistance," *Engineering ToolBox,* 2024. [Online]. Available: https://www.engineeringtoolbox.com/rolling-friction-resistance-d_1303.html.
[21] A. Rankin, M. Maimone, J. Biesiadecki, N. Patel, D. Levine, and O. Toupet, "Driving curiosity: Mars rover mobility trends during the first seven years," in *2020 IEEE aerospace conference*, 2020: IEEE, pp. 1-19.
[22] H. Gonçalves, A. Pappalettera, and G. Mantriota, "Passive Suspension Modelling for Wheeled Robots," *Journal of Field Robotics,* vol. **34**, no. 7, pp. 1225-1243, 2017.
[23] S. Thrun, W. Burgard, and D. Fox, *Probabilistic Robotics*. MIT Press, 2005.
[24] B. Li, J. Xiao, and H. Hu, "Design of a Stair-Climbing Tracking Robot with Active Link Suspension," *Autonomous Robots,* vol. **43**, no. 6, pp. 1521-1534, 2019.

[25] S. N. Armitage, "Hybrid Wheel/Track Mobility: The All-Terrain Wheelchair," *International Journal of Mechanical Engineering and Robotics Research,* vol. **5**, no. 4, pp. 215-223, 2016.